INORGANIC CHEMISTRY FRONTIERS

RESEARCH ARTICLE

View Article Online
View Journal | View Issue

Cite this: *Inorg. Chem. Front.*, 2022, **9**, 4952

Size exclusion propyne/propylene separation in an ultramicroporous yet hydrophobic metal–organic framework†

Ming-Ming Xu, Yu-Hui Liu, Xin Zhang, Hao-Tian Wang, Lin-Hua Xie * and Jian-Rong Li *

Propyne/propylene separation is important in the petrochemical industry but challenging due to their similar physical properties and close molecular sizes. Herein, we present two isoreticular ultramicroporous Zn(II)-MOFs, $Zn_2(ATZ)_2(TPDC)$ (**BUT-305**, H_2TPDC = [1,1′:3′,1″-terphenyl]-4,4″-dicarboxylic acid, HATZ = 3-amino-1,2,4-triazole) and $Zn_2(ATZ)_2(MeTPDC)$ (**BUT-306**, $H_2MeTPDC$ = 5′-methyl-[1,1′:3′,1″-terphenyl]-4,4″-dicarboxylic acid). The pore aperture of **BUT-306** (~1.6 Å) is smaller than that of **BUT-305** due to the presence of extra gate-like methyl groups in the 1D channels of the former. With a narrow and hydrophobic pore aperture, **BUT-306** exhibits high hydrophobicity and hydrolytic stability and adsorbs C_3H_4 but excludes C_3H_6 in a wide temperature range. The C_3H_6 and C_3H_4 adsorption capacities of **BUT-306** at 298 K and ~1 bar were 2.4 and 29.6 $cm^3\ g^{-1}$, respectively. Dynamic column breakthrough experiments confirmed the high capability of **BUT-306** to remove C_3H_4 from the equimolar binary gas mixture of C_3H_4 and C_3H_6. The C_3H_4/C_3H_6 separation performance of **BUT-306** was largely retained even when the binary C_3H_4/C_3H_6 gas for breakthrough experiments was pre-saturated with water vapor. In addition, the single-crystal structure of C_3H_4-loaded **BUT-306** was determined, which revealed that the adsorbed C_3H_4 molecules were located in the center of channel cavities and interacted with the MOF by multiple weak $C^{\delta-}\cdots C^{\delta+}$ dipole–dipole interactions and C–H···π interactions. This work demonstrates the high potential of an ultramicroporous, hydrophobic, and hydrolytically stable MOF in the removal of C_3H_4 from the C_3H_4/C_3H_6 gas mixture by size exclusion adsorption. The structure and gas adsorption studies shed light on the design and synthesis of new adsorbents for the separation of light hydrocarbons.

Received 30th May 2022,
Accepted 25th July 2022

DOI: 10.1039/d2qi01152b

rsc.li/frontiers-inorganic

Introduction

Propylene (C_3H_6), as a raw material of many chemical products, plays a key role in the petrochemical industry.[1] C_3H_6 is mostly produced from the cracking of large hydrocarbon molecules or crude oil in the petrochemical industry commonly accompanied by propyne (C_3H_4) as an undesirable byproduct, which can poison the catalysts for propylene polymerization.[2] Efficient removal of C_3H_4 from the C_3H_4/C_3H_6 mixture is thus of high importance. Traditional C_3H_4/C_3H_6 separation methods, such as cryogenic distillation or catalytic partial hydrogenation, suffer from high cost and high energy penalties.[3,4] The physical adsorption method based on porous materials is attractive for gas separation owing to its environmentally friendly processes and energy efficiency.[5–11] Highly efficient C_3H_4/C_3H_6 separation using traditional porous materials (such as zeolites and activated carbons) remains challenging because of highly similar physical properties, molecular sizes (C_3H_6: 4.65 × 4.16 × 6.44 $Å^3$ and C_3H_4 4.01 × 4.16 × 6.51 $Å^3$) and kinetic diameters (C_3H_6: 4.68 Å and C_3H_4: 4.76 Å) of the two hydrocarbons.[12]

As a class of newly emerged porous materials, metal–organic frameworks (MOFs)[13–20] have been widely used for gas separation owing to their structural diversity,[21–26] adjustable pore size[27–30] and designable adsorption sites.[31–37] Most reported MOFs used for C_3H_4/C_3H_6 separation are based on their open metal sites or functional groups which can strongly interact with C_3H_4. For example, the MOF-74 series (Mg, Co, Ni, and Fe-MOF-74)[38] with open metal sites and the SIFSIX series (SIFSIX-3-Ni,[39] SIFSIX-1-Cu,[40] and SIFSIX-2-Cu-i[19]) with SiF_6^{2-} anion pillars can afford high adsorption capacity and strong interaction for C_3H_4.[34] However, these MOFs allow

Beijing Key Laboratory for Green Catalysis and Separation and Department of Environmental Chemical Engineering, Faculty of Environment and Life, Beijing University of Technology, Beijing 100124, China. E-mail: xielinhua@bjut.edu.cn, jrli@bjut.edu.cn

†Electronic supplementary information (ESI) available. CCDC 2168051–2168054. For ESI and crystallographic data in CIF or other electronic format see DOI: https://doi.org/10.1039/d2qi01152b

diffusion of both C_3H_4 and C_3H_6 into their pores,[2,34,41–46] resulting in a compromised separation efficiency. In addition, the regeneration processes are relatively energy-intense due to the high affinity of these MOFs to C_3H_4. Therefore, the development of adsorbents with high performance in selective adsorption of C_3H_4 over C_3H_6 primarily relying on the molecular sieving effect would be complementary. However, among the reported MOFs, only UTSA-200 showed molecular sieving C_3H_4/C_3H_6 separation performance with a high adsorption selectivity of over 20 000.[32] In addition, stability and recyclability are also important for porous materials in gas separation applications,[47] especially when the gas mixtures to be purified contain reactive non-hydrocarbon impurities, *e.g.* water, which is ubiquitous.

Herein, we report two ultramicroporous MOFs, $Zn_2(ATZ)_2(TPDC)$ (**BUT-305**, H_2TPDC = [1,1′:3′,1″-terphenyl]-4,4″-dicarboxylic acid, HATZ = 3-amino-1,2,4-triazole) and $Zn_2(ATZ)_2(MeTPDC)$ (**BUT-306**, $H_2MeTPDC$ = 5′-methyl-[1,1′:3′,1″-terphenyl]-4,4″-dicarboxylic acid), which are 3D framework structures consisting of 2D [Zn(ATZ)] layers pillared by $TPDC^{2-}$ and $MeTPDC^{2-}$ ligands (Scheme 1), respectively. The difference between the two isoreticular MOFs is that there are extra gate-like methyl groups in the 1D channels of **BUT-306**. Owing to its narrow and hydrophobic pore aperture, **BUT-306** exhibits high hydrolytic stability, hydrophobicity, and potential in the removal of C_3H_4 from the C_3H_4/C_3H_6 mixture. In addition, the location of C_3H_4 molecules inside the pore of **BUT-306** and the host–guest interactions have been elucidated by single-crystal structural analyses.

Results and discussion

Single-crystal structures and chemical stability

As-synthesized crystals of **BUT-305** and **-306** were obtained through the solvothermal reactions of zinc salt and organic ligands (HATZ and $H_2MeTPDC$ or HATZ and $H_2MeTPDC$) in the mixture of DMF and a small amount of aqueous HBF_4 solution. The as-synthesized crystals were guest-exchanged in MeOH solvent for 3 days at 120 °C followed by heating at 120 °C for 18 hours to remove guest molecules, resulting in the formation of **BUT-305** and **-306** samples. The SCXRD measurement of **BUT-306** revealed that it crystallizes in the tetragonal *I*4/*m* space group (Table S1†) and it is isoreticular to $Zn_2(ATZ)_2(iPA)$ (H_2iPA = isophthalic acid) as reported by Chen and co-workers.[48] The 2D [Zn(ATZ)] layers are linked by the $MeTPDC^{2-}$ pillars to form a 3D pillar-layered framework with 1D channels along the crystallographic *c*-axis (Fig. 1a). The cross-sectional diameters of the channel are estimated to be 1.6 to 5.0 Å by Materials Studio.[49] It is worthy of note that the channel is highly tortuous with three types of cavities (A, B, and C), and it is divided into parts by sets of gate-like methyl groups, each set of which are from 4 neighboring $MeTPDC^{2-}$ ligands (Fig. 1b). The aperture defined by the 4 gate-like methyl groups is only about 1.6 Å in diameter. Regardless of

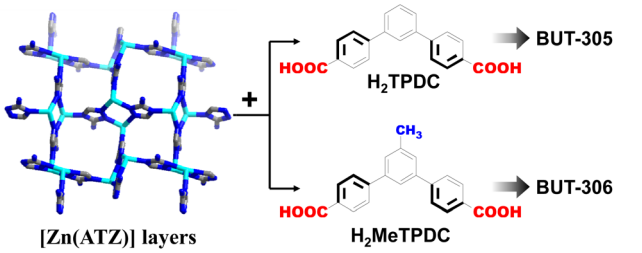

Scheme 1 The construction and building blocks of **BUT-305** and **-306**.

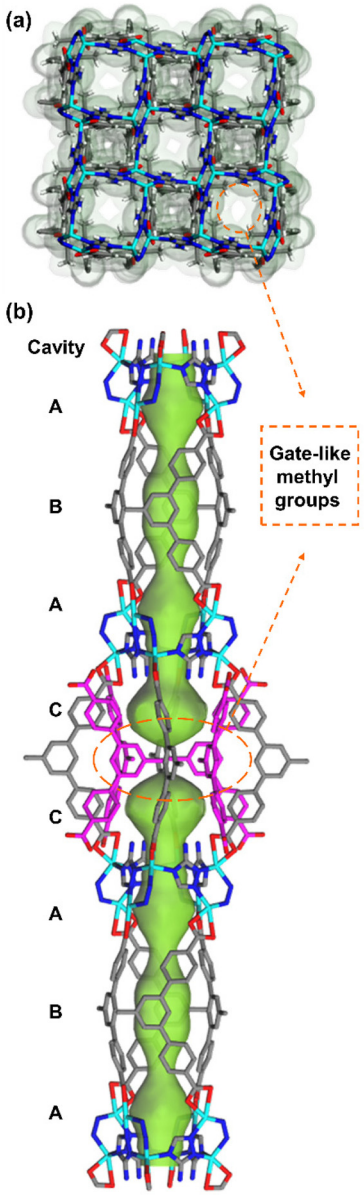

Fig. 1 The crystal structure of **BUT-306**: (a) the 3D framework view along the *c* axis and (b) side-view of the channel. Color codes: Zn, turquoise; O, red; N, blue; C, grey; H, white; and Connolly surface (probe radius 1.7 Å), green. The ligands coordinated with the metal ions on the walls of neighboring channels are shown in pink for clarity.

the small aperture size, **BUT-306** is still potentially porous as the total potential solvent area volume accounts for 23.6% of the unit cell volume of **BUT-306** and the pore volume is estimated to be 0.17 $cm^3\ g^{-1}$ by Platon.[50]

Due to the thin-plate-like shape of **BUT-305** crystals, attempts to determine their structure by SCXRD failed. The PXRD pattern of **BUT-305** resembled that of **BUT-306**, suggesting that **BUT-305** is likely isoreticular to **BUT-306** (Fig. 2a). Indexing and Pawley refinement results for the PXRD pattern of **BUT-305** showed that it also crystallizes in the same space group (*I*4/*m*) with a slightly larger unit cell relative to that of **BUT-306** (Fig. 2b and Table S2†). Due to the absence of methyl groups on the ligands of **BUT-305**, it is expected that the channels of **BUT-305** are larger than those of **BUT-306**. The difference in the channels of the two MOFs results in their distinctive gas separation performance, which will be discussed in detail below. The PXRD patterns of **BUT-305** and **-306** samples well matched the simulated one from the single-crystal structure of **BUT-306** (Fig. 2a), which confirmed that the prepared **BUT-305** and **-306** samples were pure phases. In addition, the PXRD measurements showed that the highly crystalline structures of **BUT-305** and **-306** samples remained essentially unchanged after they were treated with methanol at 120 °C for 3 days (Fig. S1†) or treated with water at room temperature for 24 hours (Fig. 2a), demonstrating their high hydrolytic stability.

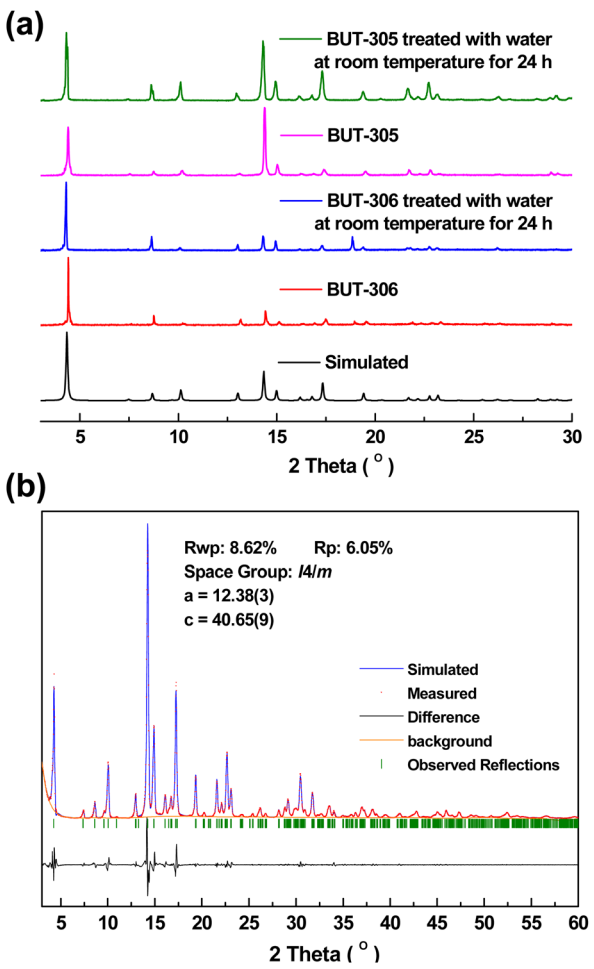

Fig. 2 (a) The PXRD patterns of **BUT-305** and **BUT-306**. (b) The results of Pawley refinement for the PXRD data of **BUT-305**. For comparison, the space group and cell parameters of **BUT-306** are as follows: *I*4/*m*, *a* = 12.3420(2) Å, and *c* = 40.6826(9) Å.

Adsorption studies

To verify the accessibility of their pores, N_2 adsorption isotherms of **BUT-305** and **-306** were recorded at 77 K (Fig. S2†). Although the calculated pore volumes of the two MOFs are over 0.17 $cm^3\ g^{-1}$, type I N_2 adsorption isotherms were not obtained. The N_2 uptake at $P/P_0 \approx 1$ was only 1.2 $cm^3\ g^{-1}$ for **BUT-306**, suggesting that N_2 molecules could not diffuse into its channels at 77 K. The N_2 uptake of **BUT-305** gradually increased as the pressure is increased with an N_2 uptake of 77.1 $cm^3\ g^{-1}$ at $P/P_0 \approx 1$, which might result from the comparable size of the N_2 molecule and the pore of **BUT-305**. The CO_2 adsorption isotherms of **BUT-305** and **-306** at 195 K were then recorded. As shown in Fig. S3,† the two MOFs showed an abrupt increase in CO_2 uptake (to ~70 $cm^3\ g^{-1}$) at low pressures ($P/P_0 < 0.1$). At higher pressures, the CO_2 uptake of **BUT-306** only slightly increased, while that of **BUT-305** increased to 193 $cm^3\ g^{-1}$ at $P/P_0 \approx 1$ by two additional stepwise increases, indicating the presence of some difference in the pore size, shape and/or flexibility of the two MOFs. According to the adsorption data at low pressures, the BET surface areas of **BUT-305** and **-306** were estimated to be 351 and 305 $m^2\ g^{-1}$, respectively. Water adsorption isotherms were also recorded for the MOFs at 298 K. Type III water adsorption isotherms were obtained for both MOFs (Fig. 3a and S4†), and the water uptakes at $P/P_0 \approx 1$ were 160 and 80 $cm^3\ g^{-1}$ for **BUT-305** and **BUT-306**, respectively. These results indicated that the two MOFs were capable of accommodating small molecules and their pore surface was relatively hydrophobic.

Encouraged by the high stability, accessible porosity and small pore apertures of the two MOFs, we explored their performances in light hydrocarbon separations. Adsorption isotherms for C_2H_2, C_2H_4, C_2H_6, C_3H_4, C_3H_6, and C_3H_8 were recorded at 298 K, as shown in Fig. S5.† The adsorption capacities of **BUT-305** for C_2H_2, C_2H_4 and C_2H_6 at ~1 bar were similar (42.3–44.6 $cm^3\ g^{-1}$), and its adsorption capacities for C_3H_4 (44.4 $cm^3\ g^{-1}$) and C_3H_6 (43.9 $cm^3\ g^{-1}$) at ~1 bar were also close, but that for C_3H_8 (33.8 $cm^3\ g^{-1}$) was lower. These results suggested that all these hydrocarbons could enter the pore of **BUT-305**, and the differences in adsorption capacities of **BUT-305** for these hydrocarbons were not profound. In contrast, strong size exclusion effects were observed in the hydrocarbon adsorption isotherms of **BUT-306**. For C_2 hydrocarbons, the uptake of **BUT-306** for C_2H_2 (36.6 $cm^3\ g^{-1}$) or C_2H_4 (30.3 $cm^3\ g^{-1}$) was obviously higher than that for C_2H_6 (11.0 $cm^3\ g^{-1}$) at ~1 bar. Moreover, the uptakes of **BUT-306** for C_3H_6 (2.4 $cm^3\ g^{-1}$) and C_3H_8 (0.33 $cm^3\ g^{-1}$) at ~1 bar were nearly negligible (Fig. S5d†), but a type I-like C_3H_4 adsorption isotherm was obtained for **BUT-306** with a relatively high

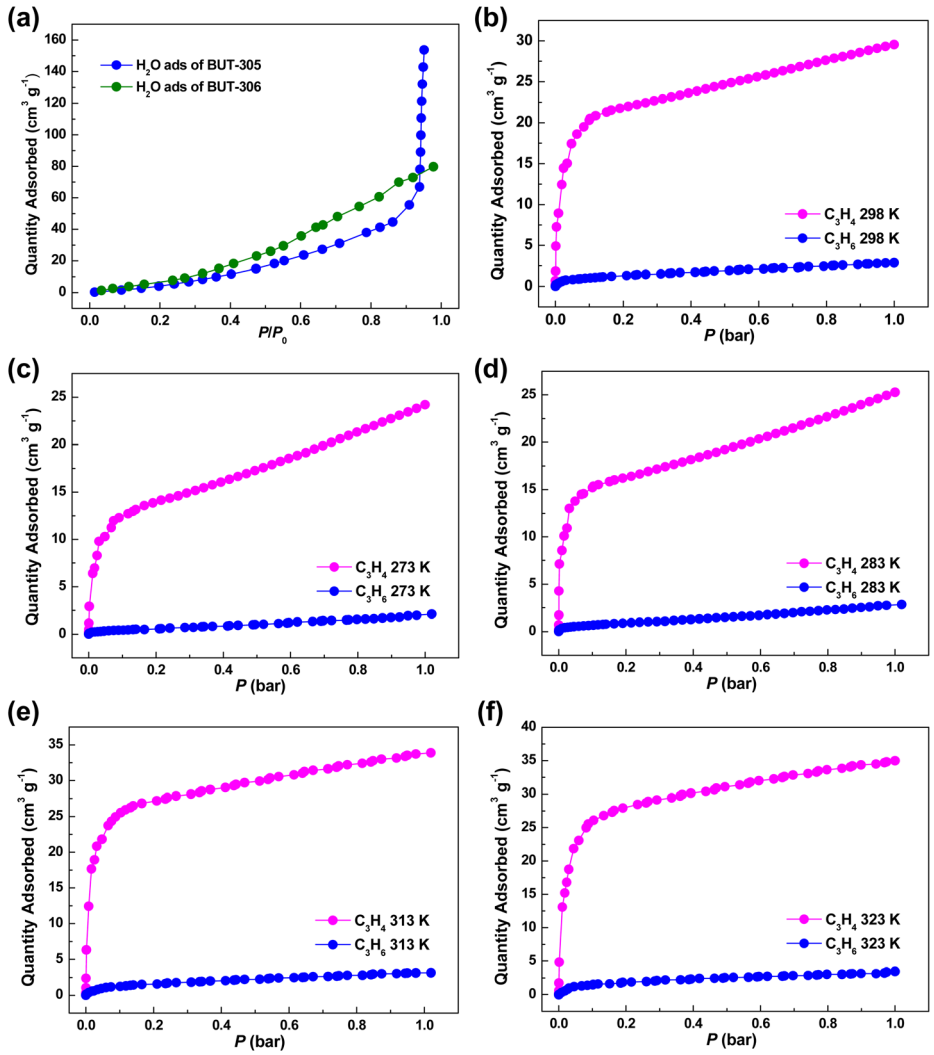

Fig. 3 Adsorption and separation performance of **BUT-306**. (a) The H_2O adsorption isotherms of **BUT-305** and **-306** at 298 K. Single-component C_3H_4 and C_3H_6 adsorption isotherms of **BUT-306** at (b) 298 K, (c) 273 K, (d) 283 K (e) 313 K and (f) 323 K, respectively.

uptake of 29.6 $cm^3\ g^{-1}$ at ~1 bar (Fig. 3b and S6†), indicating its potential in the removal of C_3H_4 from the C_3H_4/C_3H_6 mixture. Although the C_3H_4 adsorption capacity of **BUT-306** is lower than those of some reported MOFs under similar conditions, *e.g.*, SIFSIX-2-Cu-i (84.4 $cm^3\ g^{-1}$), UTSA-200 (80.2 $cm^3\ g^{-1}$) and ELM-12 (62.1 $cm^3\ g^{-1}$), **BUT-306** hardly permits the entrance of C_3H_6 molecules into its pores. The C_3H_6 adsorption capacity of **BUT-306** was only 2.4 $cm^3\ g^{-1}$ at ~1 bar and 298 K, significantly lower than those of the reported MOFs (Table S3†),[32,51,52] including SIFSIX-2-Cu-i (58.9 $cm^3\ g^{-1}$), UTSA-200 (26.9 $cm^3\ g^{-1}$), and ELM-12 (32.0 $cm^3\ g^{-1}$). The size exclusion effects of **BUT-306** on the adsorption of C_3H_4 over C_3H_6 should be related to the small apertures defined by gate-like methyl groups in its 1D channels.

For a better comparison, the uptake ratios of **BUT-306** for C_3H_4 over C_3H_6 at 0.99 bar or at 0.01/0.99 bars (0.01 bar for C_3H_4 and 0.99 for C_3H_6) and 298 K were calculated, being 10.75 and 3.67, respectively, which are much higher than those of the reported porous materials (1.05–3.07 at 0.99 bar; 0.03–2.49 at 0.01/0.99 bars) under similar conditions (Table S3†). Furthermore, ideal adsorbed solution theory (IAST) was used to predict the C_3H_4/C_3H_6 adsorption selectivity of **BUT-306**. Assuming the gas mixture with C_3H_4/C_3H_6 ratios (v/v) of 1 : 1, 1 : 9 and 1 : 99, the IAST C_3H_4/C_3H_6 adsorption selectivities of **BUT-306** at ~1 bar and 298 K were calculated to be 636, 717, and 989, respectively (Fig. S7†).

To explore the adsorption performances of **BUT-306** for C_3H_4 and C_3H_6 in a broader temperature range, C_3H_4 and C_3H_6 adsorption isotherms were measured at 273, 283, 313 and 323 K, respectively. As shown in Fig. 3c–f, type I-like adsorption isotherms were obtained for C_3H_4 at all four temperatures, and the adsorption capacities at ~1 bar were all over 25 $cm^3\ g^{-1}$, while the C_3H_6 uptakes were all relatively low (<5 $cm^3\ g^{-1}$). It is indicated that the size exclusion adsorption behavior of **BUT-306** is not highly sensitive to the temperature. The adsorption capacity of **BUT-306** for C_3H_4 or C_3H_6 gradually

increased as the temperature increased from 273 to 323 K. For example, the C_3H_4 uptake at ~1 bar increased from 24.2 cm^3 g^{-1} at 273 K to 35.0 cm^3 g^{-1} at 323 K. The adsorption data at these temperatures were further verified by repeated adsorption isotherm measurements (Fig. S8†). It is not common because physisorption is essentially exothermic, and the adsorption capacities at a certain equilibrium pressure should decrease when increasing the adsorption temperature for typical physical adsorption adsorbents. The abnormal adsorption behavior suggests the existence of structural flexibility in **BUT-306**.[53,54] To verify this, SCXRD measurements were carried out for the same one single crystal of **BUT-306** at 273 K, 313 K and 298 K, respectively. As shown in Fig. S9 and Table S1,† the unit cell parameters were nearly unchanged and no obvious structural change was observed during varying the measurement temperatures, indicating that the structural flexibility was induced by the adsorption of hydrocarbons rather than the change of temperature. Otherwise, according to the static equilibrium crystal structure of **BUT-306**, the narrowest pore aperture is too small (diameter: 1.6 Å) to let the hydrocarbon molecules diffuse into the channels. The increase of measurement temperature should be beneficial for the diffusion of C_3H_4 molecules into **BUT-306** as there is an energy barrier between the guest-free state and the guest-included state originating from the structural flexibility of **BUT-306**, which leads to the uncommon adsorption behavior of **BUT-306** as mentioned above.

For a better understanding of the C_3H_4 adsorption process of **BUT-306**, the single-crystal structure of C_3H_4-loaded **BUT-306** was determined. A single crystal of **BUT-306** preheated at 50 °C under an N_2 atmosphere for 6 hours was exposed to the atmosphere of C_3H_4 at ambient pressure and temperature for 30 minutes to load the hydrocarbon molecules, which was then mounted on a single-crystal X-ray diffractometer under a low-temperature N_2 flow bath (200 K) for data collection. Structure determination and refinement results revealed that the framework of **BUT-306** was essentially unchanged after C_3H_4 loading (Fig. S9 and Table S1†) and two crystallographically independent C_3H_4 molecules were found inside its channels. As the framework was retained, the narrowest channel apertures defined by the methyl groups of $MeTPDC^{2-}$ ligands kept unchanged after C_3H_4 loading, indicating that there was a transient structural variation to open the gate-like apertures when C_3H_4 molecules diffused into the channels. The transient gate-opening might have resulted from the swing or distortion of the $MeTPDC^{2-}$ ligands.

The two types of C_3H_4 molecules are located inside cavities A and B with a linear molecular shape along the 4-fold rotation axis, respectively (Fig. 4a). The C–C triple bond and single bond of the C_3H_4 molecule located at cavity A (C_3H_4-A) are 1.08 (8) and 1.54(8) Å, respectively. The C_3H_4 molecule located at cavity B (C_3H_4-B) is normal to the reflection plane crossing its center C atom. Due to the symmetry-imposed disorder, the two C–C bonds of C_3H_4-B are same in length, being 1.24(8) Å, close to the average length of a C–C triple bond and a C–C single bond. Occupations of the two C_3H_4 molecules were set

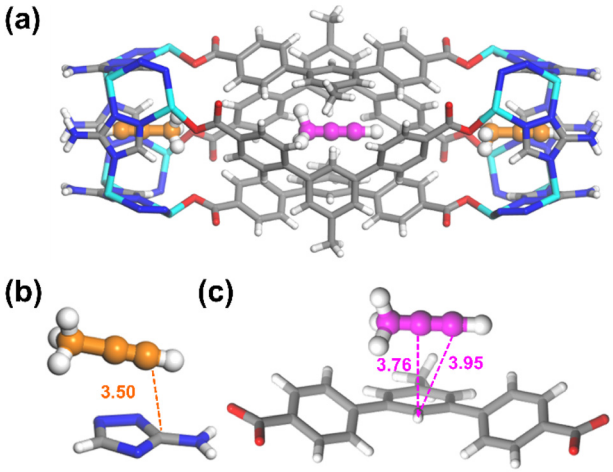

Fig. 4 (a) The two types of C_3H_4 adsorption sites in the cavities of **BUT-306**. The interaction between the **BUT-306** framework and the C_3H_4 molecules located in cavity A (b) and in cavity B (c). Color codes: Zn, turquoise; O, red; N, blue; C, grey; and H, white. For clarity, the C atoms of C_3H_4-A and C_3H_4-B are in gold and pink colors, respectively.

to be 20%, and no geometrical restraints were used in the structure refinements. The C_3H_4 molecules are confined inside the cavities by multiple weak host–guest interactions with the framework. Specifically, the distance between the terminal sp-hybridized C atom (with a negative charge) of C_3H_4-A and the 3-position C atoms (with a positive charge) of four neighboring ATZ^- ligands on the channel walls is 3.50 Å (Fig. 4b), slightly larger than the van der Waals radii of two C atoms (1.7 × 2 Å), indicating the presence of weak $C^{\delta-}\cdots C^{\delta+}$ dipole–dipole interactions. In addition, there are fourfold weak C–H···π interactions between C_3H_4-B and the aromatic H atoms of four neighboring $MeTPDC^{2-}$ ligands ($C_{C_3H_4}\cdots H$ distances: 3.76, 3.95 Å; <C–H···C angles: 85.9, 86.1°) (Fig. 4c). Though every single interaction is weak, the overall interactions between C_3H_4 and MOF should be moderate because each C_3H_4 molecule is interacting with four neighboring channel walls simultaneously. Assuming that the two adsorption sites are fully occupied, the calculated C_3H_4 uptake of **BUT-306** is 26.8 cm^3 g^{-1}, which is slightly lower than the experimentally observed uptake (29.6 cm^3 g^{-1}) at ~1 bar and 298 K. It is noteworthy that C_3H_4 uptake of **BUT-306** at ~1 bar gradually increased from 24.2 to 35.0 cm^3 g^{-1} as the temperature increased from 273 to 323 K. This fact suggests that the adsorbed C_3H_4 molecules could be also located inside the cavity C besides cavities A and B. When each of the cavities is occupied by one C_3H_4 molecule, the calculated C_3H_4 uptake of **BUT-306** is 35.7 cm^3 g^{-1}, close to the uptake (35.0 cm^3 g^{-1}) observed at ~1 bar and 323 K, further justifying the assignment of adsorption sites.

Dynamic column breakthrough studies

Dynamic column breakthrough experiments of a binary gas of C_3H_4/C_3H_6 (1 : 1, v/v) were carried out at ambient pressure and temperature to further evaluate the separation performance of **BUT-306** for a real gas mixture. As the binary gas flowed

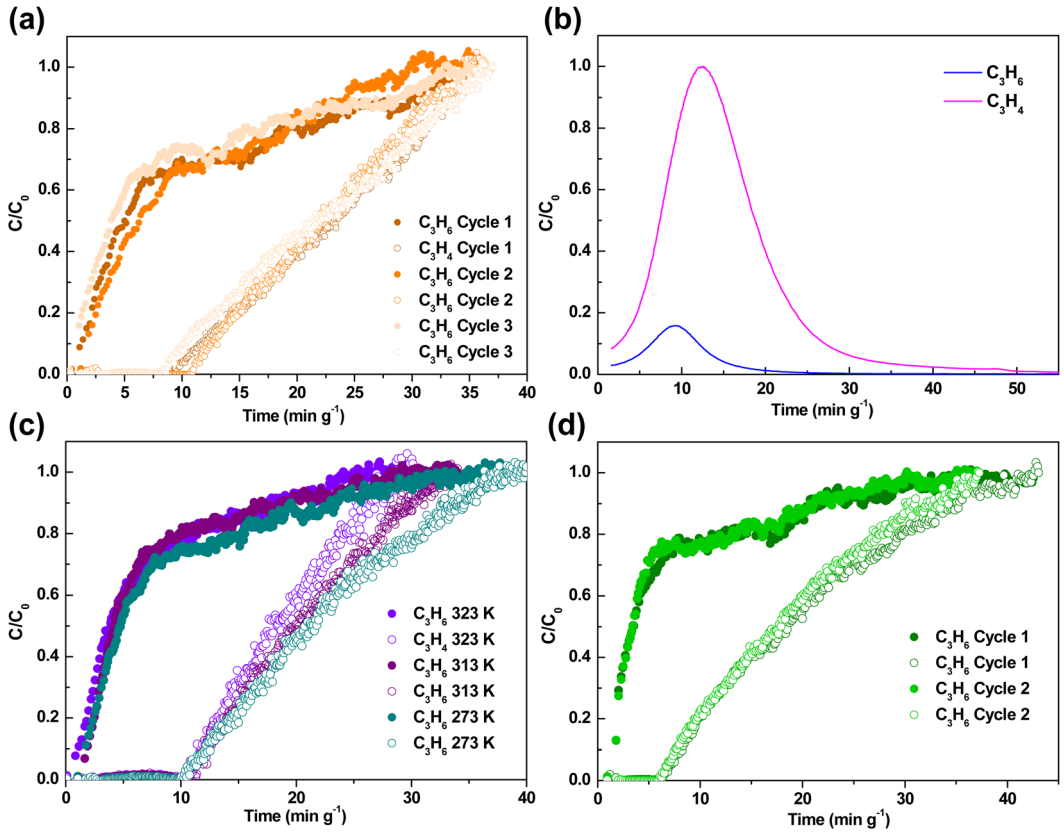

Fig. 5 Dynamic column breakthrough curves of **BUT-306** for a binary C_3H_4/C_3H_6 (1 : 1, v/v) gas (a) at room temperature, (c) at 273, 313 and 323 K, and (d) under RH ≈ 100% at room temperature, respectively. (b) The MS signal peaks of C_3H_4 and C_3H_6 at the outlet when the MOF column was purged with a He gas flow at 393 K after a breakthrough test at room temperature.

through the column packed with **BUT-306**, purified C_3H_6 was detected in the outlet of the column, while C_3H_4 was trapped in the column until the retention time reached ~10 min g^{-1} (Fig. 5a). After saturation of gas adsorption, the MOF was regenerated at 393 K under a He gas flow. Meanwhile, the gas eluted from the outlet was monitored. As shown in Fig. 5b, the peak area of desorbed C_3H_4 was significantly larger than that of desorbed C_3H_6, indicating the high adsorption selectivity of C_3H_4 over C_3H_6. The dynamic C_3H_4 productivity is estimated to be 0.87 mol kg^{-1} h^{-1} with a purity of 90.3% by analyzing the breakthrough and desorption curves. It is important to note that during the C_3H_4/C_3H_6 separation process, the fewer the C_3H_6 molecules the adsorbent adsorbs, the higher the C_3H_6 purification productivity and efficiency. The **BUT-306** sample was regenerated and used for the C_3H_4/C_3H_6 breakthrough experiment for two more cycles, and its separation performance essentially unchanged (Fig. 5a), which indicated that **BUT-306** could be fully regenerated for repeated use in the removal of C_3H_4 from the C_3H_4/C_3H_6 mixture. Breakthrough experiments were also carried out at 273, 313 and 323 K. As shown in Fig. 5c, the final retention times of C_3H_4 nearly kept unchanged after varying the measurement temperatures. Since **BUT-306** shows high hydrolytic stability and hydrophobicity, the effect of water vapor on its C_3H_4/C_3H_6 separation performance was also investigated. The breakthrough experiments were carried out with the binary C_3H_4/C_3H_6 gas pre-saturated with water vapor (RH ≈ 100% at ambient temperature). It was found that the separation performance of **BUT-306** was not lost under such a high humidity (Fig. 5d). The retention time of C_3H_4 was ~6 min g^{-1}, about 60% of that under dry conditions. The breakthrough experiment under humid conditions was repeated after regeneration of the MOF, and the two breakthrough curves obtained from the two successive runs well overlapped, suggesting the high and stable separation performance of **BUT-306** due to its ultramicroporous, stable and hydrophobic nature.

Conclusions

Two new MOFs **BUT-305** and **-306** with isoreticular ultramicroporous structures have been synthesized. The pore aperture of **BUT-306** (~1.6 Å) is smaller than that of **BUT-305** due to the presence of extra gate-like methyl groups in the channels of the former. This structural feature endows **BUT-306** with a high adsorption selectivity of C_3H_4 over C_3H_6. The C_3H_6 and C_3H_4 adsorption capacities of **BUT-306** at 298 K and ~1 bar were 2.4 and 29.6 cm^3 g^{-1}, respectively, indicating a size exclu-

sion adsorption behavior. Based on the single-component gas adsorption isotherms, the IAST C_3H_4/C_3H_6 adsorption selectivity at 298 K and 1 bar was calculated to be 636 for an equimolar mixture of C_3H_4 and C_3H_6. Dynamic column breakthrough experiments of a binary gas confirmed the high capability of **BUT-306** to remove C_3H_4 from a real C_3H_4/C_3H_6 mixture. Thanks to its high hydrolytic stability and hydrophobicity, the C_3H_4/C_3H_6 separation performance of **BUT-306** was largely retained even when the binary C_3H_4/C_3H_6 gas for breakthrough experiments was pre-saturated with water vapor. In addition, the single-crystal structure of C_3H_4-loaded **BUT-306** revealed that the adsorbed C_3H_4 molecules were located in the center of channel cavities and interacted with the MOF by multiple weak $C^{\delta-}\cdots C^{\delta+}$ dipole–dipole interactions and C–H···π interactions. In short, this study reports an ultramicroporous, hydrophobic, and hydrolytically stable MOF with high performance in the removal of C_3H_4 from a C_3H_4/C_3H_6 gas mixture by size exclusion adsorption. Its structure and gas adsorption studies shed light on the design and synthesis of new adsorbents for light hydrocarbon separations.

Experimental section

Materials and characterization

All general reagents and solvents (AR grade) were purchased commercially and used directly. The single-crystal X-ray diffraction data (SCXRD) of **BUT-306** (at 273, 298, and 313 K) and C_3H_4-loaded **BUT-306** (at 200 K) were collected on a Rigaku Supernova CCD diffractometer equipped with a graphite-monochromatic enhanced Cu-Kα radiation source (λ = 1.54184 Å). These SCXRD data for **BUT-306** have been deposited in the Cambridge Crystallographic Data Centre (CCDC accession numbers: 2168051–2168054†). The PXRD pattern (2θ range: 3–60°) of **BUT-305** was measured with a Bruker D8 Advance X-ray powder diffractometer and Pawley refinement[55] of the PXRD data was performed in Materials Studio. The peak profiles, background, zero-shift, asymmetry, and unit cell parameters were together refined. The final Pawley refinement results are shown in Fig. 2a and Table S2.† The simulated PXRD pattern was obtained from single-crystal data of **BUT-306** *via* the Mercury program.[56] The other experimental PXRD data were recorded on a Rigaku SmartLab3 X-ray powder diffractometer that was equipped with a Cu sealed tube (λ = 1.54178 Å) with a scanning rate of 10° min^{-1}. The gas sorption measurements were performed using a Micromeritics ASAP 2020 surface area and pore analyzer.

Synthesis and activation

A mixture of HATZ (18 mg), H_2MeTPDC (30 mg) or H_2MeTPDC (32 mg) and $Zn(CH_3COO)_2\cdot$(90 mg) was dissolved in 18 mL of DMF and placed in a 20 mL glass vial containing 720 μL of 48% aqueous HBF_4 solution. Then the mixture sealed in the vial was heated in an oven to 120 °C for 48 hours and the as-synthesized colorless crystals of **BUT-305** or **-306** were obtained. After the solution was cooled, the crystals were collected and washed several times with CH_3OH and dried under vacuum.

The as-synthesized samples of the two MOFs were first soaked in fresh DMF at 60 °C for 12 hours to remove the excess organic ligands and metal salts. Then, these samples were immersed in MeOH for 3 days at 120 °C. In order to ensure the activation effect, the extract was replaced with fresh methanol three times a day. Finally, the samples in MeOH were collected and dried at 120 °C under vacuum for 18 hours for gas adsorption measurements.

Gas adsorption measurements

The N_2 adsorption isotherms of **BUT-305** and **-306** were measured at 77 K, while their water adsorption isotherms were recorded at 298 K. Single-component gas (C_2H_2, C_2H_4, C_2H_6, C_3H_4, C_3H_6, and C_3H_8) adsorption isotherms of the two MOFs were measured at 298 K. In addition, the C_3H_4 and C_3H_6 adsorption isotherms of **BUT-306** were also recorded at 273, 283, 313 and 323 K, respectively. The C_3H_4 and C_3H_6 adsorption isotherms of **BUT-306** at 298 were fit by the Langmuir–Freundlich equation, respectively (Fig. S10†). Then, based on the single-component gas adsorption isotherms of **BUT-306** for C_3H_4 and C_3H_6 at 298 K, ideal adsorbed solution theory (IAST) was used for the prediction of adsorption equilibria of the binary gas mixtures.[57] The selectivity of preferential adsorption of component 1 (C_3H_4) over 2 (C_3H_6) in a mixture containing 1 and 2 can be formally defined as an equation (eqn (1)), where q_1 and q_2 are the absolute loadings at the partial pressures p_1 and p_2, respectively. To calculate the C_3H_4/C_3H_6 adsorption selectivity of **BUT-306** for gas separation, the gas mixture composition is assumed to be 1 : 99, 1 : 9 and 1 : 1, respectively.

$$S_{1,2} = \frac{q_1/q_2}{p_1/p_2} \quad (1)$$

Breakthrough experiments

The breakthrough experiments for the binary C_3H_4/C_3H_6 gas mixture (1 : 1, v/v) were carried out using a setup as shown in Fig. S11.† A powder sample of **BUT-306** (330 mg) was packed in a quartz tube (o.d. 6 mm, i.d. 3 mm, and length 150 mm). The temperature of the MOF sample packed in the quartz tube was controlled by a heating jacket (298, 313, 323, and 393 K) or by an ice/water bath (273 K). The gas mixture flow rate was set to be 2 mL min^{-1} by the mass flow controllers (MFC). The outlet gas compositions from the column were determined continuously using a mass spectrometer (MS, Hiden, HPR-20). For the breakthrough experiments with a humid gas mixture, the C_3H_4/C_3H_6 mixture was pre-saturated with water vapor (relative humidity (RH) ≈ 100% at room temperature) by bubbling it through deionized water before it passed through the MOF column. The sample was regenerated for repeated tests under a He flow for 4 hours at 393 K.

Conflicts of interest

The authors declare no conflict of interest.

Acknowledgements

We would like to acknowledge the financial support from the National Natural Science Foundation of China (No. 22038001 and 51621003).

References

1 M. F. Friedrich, M. Lucas and P. Claus, Selective hydrogenation of propyne on a solid Pd/Al_2O_3 catalyst modified with ionic liquid layer (SCILL), *Catal. Commun.*, 2017, **88**, 73–76.
2 L. Li, R.-B. Lin, R. Krishna, X. Wang, B. Li, H. Wu, J. Li, W. Zhou and B. Chen, Flexible-Robust Metal-Organic Framework for Efficient Removal of Propyne from Propylene, *J. Am. Chem. Soc.*, 2017, **139**, 7733–7736.
3 B. Bridier, N. López and J. Pérez-Ramírez, Partial hydrogenation of propyne over copper-based catalysts and comparison with nickel-based analogues, *J. Catal.*, 2010, **269**, 80–92.
4 R. P. Lively and D. S. Sholl, Seven chemical separations to change the world, *Nature*, 2016, **532**, 435–437.
5 J. Jiang, Z. Lu, M. Zhang, J. Duan, W. Zhang, Y. Pan and J. Bai, Higher Symmetry Multinuclear Clusters of MOFs for Highly Selective CO_2 Capture, *J. Am. Chem. Soc.*, 2018, **140**, 17825–17829.
6 K. Sumida, D. L. Rogow, J. A. Mason, T. M. McDonald, E. D. Bloch, Z. R. Herm, T.-H. Bae and J. R. Long, Carbon Dioxide Capture in Metal-Organic Frameworks, *Chem. Rev.*, 2012, **112**, 724–781.
7 L.-H. Xie and M. P. Suh, High CO_2-Capture Ability of a Porous Organic Polymer Bifunctionalized with Carboxy and Triazole Groups, *Chem. – Eur. J.*, 2013, **19**, 11590–11597.
8 K.-J. Chen, H. S. Scott, D. G. Madden, T. Pham, A. Kumar, A. Bajpai, M. Lusi, K. A. Forrest, B. Space, J. J. Perry and M. J. Zaworotko, Benchmark C_2H_2/CO_2 and CO_2/C_2H_2 Separation by Two Closely Related Hybrid Ultramicroporous Materials, *Chem*, 2016, **1**, 753–765.
9 H. G. Hao, Y. F. Zhao, D. M. Chen, J. M. Yu, K. Tan, S. Ma, Y. Chabal, Z. M. Zhang, J. M. Dou, Z. H. Xiao, G. Day, H. C. Zhou and T. B. Lu, Simultaneous Trapping of C2H2 and C2H6 from a Ternary Mixture of C2H2 /C2H4 /C2H6 in a Robust Metal-Organic Framework for the Purification of C2H4, *Angew. Chem., Int. Ed.*, 2018, **57**, 16067–16071.
10 K. Li, D. H. Olson, J. Seidel, T. J. Emge, H. Gong, H. Zeng and J. Li, Zeolitic imidazolate frameworks for kinetic separation of propane and propene, *J. Am. Chem. Soc.*, 2009, **131**, 10368–10369.
11 Z. Zhang, B. Tan, P. Wang, X. Cui and H. Xing, Highly efficient separation of linear and branched C4 isomers with a tailor-made metal–organic framework, *AIChE J.*, 2020, **66**, e16236.
12 P. Samaddar, Y.-S. Son, D. C. W. Tsang, K.-H. Kim and S. Kumar, Progress in graphene-based materials as superior media for sensing, sorption, and separation of gaseous pollutants, *Coord. Chem. Rev.*, 2018, **368**, 93–114.
13 H.-C. J. Zhou and S. Kitagawa, Metal-Organic Frameworks (MOFs), *Chem. Soc. Rev.*, 2014, **43**, 5415.
14 Y. Liu, H. Dong, F. Hu and Y. S. Zhao, Metal-organic framework microlasers, *Sci. Bull.*, 2017, **62**, 3–4.
15 W. G. Cui, T. L. Hu and X. H. Bu, Metal-Organic Framework Materials for the Separation and Purification of Light Hydrocarbons, *Adv. Mater.*, 2020, **32**, e1806445.
16 W. Fan, X. Zhang, Z. Kang, X. Liu and D. Sun, Isoreticular chemistry within metal–organic frameworks for gas storage and separation, *Coord. Chem. Rev.*, 2021, **443**, 213968–214024.
17 R.-B. Lin, S. Xiang, W. Zhou and B. Chen, Microporous Metal-Organic Framework Materials for Gas Separation, *Chem*, 2020, **6**, 337–363.
18 M. R. Tchalala, P. M. Bhatt, K. N. Chappanda, S. R. Tavares, K. Adil, Y. Belmabkhout, A. Shkurenko, A. Cadiau, N. Heymans, G. De Weireld, G. Maurin, K. N. Salama and M. Eddaoudi, Fluorinated MOF platform for selective removal and sensing of SO_2 from flue gas and air, *Nat. Commun.*, 2019, **10**, 1328–1338.
19 P. Nugent, Y. Belmabkhout, S. D. Burd, A. J. Cairns, R. Luebke, K. Forrest, T. Pham, S. Ma, B. Space, L. Wojtas, M. Eddaoudi and M. J. Zaworotko, Porous materials with optimal adsorption thermodynamics and kinetics for CO_2 separation, *Nature*, 2013, **495**, 80–84.
20 V. F. Martins, A. M. Ribeiro, M. G. Plaza, J. C. Santos, J. M. Loureiro, A. F. Ferreira and A. E. Rodrigues, Gas-phase simulated moving bed: Propane/propylene separation on 13X zeolite, *J. Chromatogr. A*, 2015, **1423**, 136–148.
21 F. ZareKarizi, M. Joharian and A. Morsali, Pillar-layered MOFs: functionality, interpenetration, flexibility and applications, *J. Mater. Chem. A*, 2018, **6**, 19288–19329.
22 C. Yu, Q. Ding, J. Hu, Q. Wang, X. Cui and H. Xing, Selective capture of carbon dioxide from humid gases over a wide temperature range using a robust metal–organic framework, *Chem. Eng. J.*, 2021, **405**, 126937–126944.
23 T. Liu, H. Cui, X. Zhang, Z. Y. Zhang, R. B. Lin, B. Liang, J. Zhang, D. Li and B. Chen, Doubly Interpenetrated Metal-Organic Framework of pcu Topology for Selective Separation of Propylene from Propane, *ACS Appl. Mater. Interfaces*, 2020, **12**, 48712–48717.
24 X. Wang, R. Krishna, L. Li, B. Wang, T. He, Y.-Z. Zhang, J.-R. Li and J. Li, Guest-dependent pressure induced gate-opening effect enables effective separation of propene and propane in a flexible MOF, *Chem. Eng. J.*, 2018, **346**, 489–496.
25 L. Yang, X. Cui, Q. Ding, Q. Wang, A. Jin, L. Ge and H. Xing, Polycatenated Molecular Cage-Based Propane Trap for Propylene Purification with Recorded Selectivity, *ACS Appl. Mater. Interfaces*, 2020, **12**, 2525–2530.
26 L. Yu, X. Han, H. Wang, S. Ullah, Q. Xia, W. Li, J. Li, I. da Silva, P. Manuel, S. Rudic, Y. Cheng, S. Yang, T. Thonhauser and J. Li, Pore Distortion in a Metal-Organic Framework for Regulated Separation of Propane and Propylene, *J. Am. Chem. Soc.*, 2021, **143**, 19300–19305.

27 Z. Zhang, Q. Ding, S. B. Peh, D. Zhao, J. Cui, X. Cui and H. Xing, Mechano-assisted synthesis of an ultramicroporous metal-organic framework for trace CO_2 capture, *Chem. Commun.*, 2020, **56**, 7726–7729.

28 B. Liang, X. Zhang, Y. Xie, R. B. Lin, R. Krishna, H. Cui, Z. Li, Y. Shi, H. Wu, W. Zhou and B. Chen, An Ultramicroporous Metal-Organic Framework for High Sieving Separation of Propylene from Propane, *J. Am. Chem. Soc.*, 2020, **142**, 17795–17801.

29 R. B. Lin, L. Li, H. Wu, H. Arman, B. Li, R. G. Lin, W. Zhou and B. Chen, Optimized Separation of Acetylene from Carbon Dioxide and Ethylene in a Microporous Material, *J. Am. Chem. Soc.*, 2017, **139**, 8022–8028.

30 H. Wang, X. Dong, V. Colombo, Q. Wang, Y. Liu, W. Liu, X. L. Wang, X. Y. Huang, D. M. Proserpio, A. Sironi, Y. Han and J. Li, Tailor-Made Microporous Metal-Organic Frameworks for the Full Separation of Propane from Propylene Through Selective Size Exclusion, *Adv. Mater.*, 2018, **30**, e1805088.

31 Z. Jiang, L. Fan, P. Zhou, T. Xu, S. Hu, J. Chen, D.-L. Chen and Y. He, An aromatic-rich cage-based MOF with inorganic chloride ions decorating the pore surface displaying the preferential adsorption of C_2H_2 and C_2H_6 over C_2H_4, *Inorg. Chem. Front.*, 2021, **8**, 1243–1252.

32 L. Li, H.-M. Wen, C. He, R.-B. Lin, R. Krishna, H. Wu, W. Zhou, J. Li, B. Li and B. Chen, A Metal-Organic Framework with Suitable Pore Size and Specific Functional Sites for the Removal of Trace Propyne from Propylene, *Angew. Chem., Int. Ed.*, 2018, **57**, 15183–15188.

33 X.-Q. Wu, J.-H. Liu, T. He, P.-D. Zhang, J. Yu and J.-R. Li, Understanding how pore surface fluorination influences light hydrocarbon separation in metal–organic frameworks, *Chem. Eng. J.*, 2021, **407**, 127183–127192.

34 L. Yang, X. Cui, Q. Yang, S. Qian, H. Wu, Z. Bao, Z. Zhang, Q. Ren, W. Zhou, B. Chen and H. Xing, Highly Efficient Removal of Propyne from Propylene with Anion-Pillared Ultramicroporous Materials, *Adv. Mater.*, 2018, **30**, 1705374–1705382.

35 Z. Zhang, Q. Ding, X. Cui, X. M. Jiang and H. Xing, Fine-Tuning and Selective-Binding within an Anion-Functionalized Ultramicroporous Metal-Organic Framework for Efficient Olefin/Paraffin Separation, *ACS Appl. Mater. Interfaces*, 2020, **12**, 40229–40235.

36 B. Yu, S. Geng, H. Wang, W. Zhou, Z. Zhang, B. Chen and J. Jiang, A Solid Transformation into Carboxyl Dimers Based on a Robust Hydrogen–Bonded Organic Framework for Propyne/Propylene Separation, *Angew. Chem.*, 2021, **133**, 26146–26152.

37 R. Das, S. S. Dhankhar and C. M. Nagaraja, Construction of a bifunctional Zn(II)–organic framework containing a basic amine functionality for selective capture and room temperature fixation of CO_2, *Inorg. Chem. Front.*, 2020, **7**, 72–81.

38 S. R. Caskey, A. G. Wong-Foy and A. J. Matzger, Dramatic Tuning of Carbon Dioxide Uptake via Metal Substitution in a Coordination Polymer with Cylindrical Pores, *J. Am. Chem. Soc.*, 2008, **130**, 10870–10871.

39 A. Kumar, D. G. Madden, M. Lusi, K. J. Chen, E. A. Daniels, T. Curtin, J. J. T. Perry and M. J. Zaworotko, Direct Air Capture of CO_2 by Physisorbent Materials, *Angew. Chem., Int. Ed.*, 2015, **54**, 14372–14377.

40 S. D. Burd, S. Ma, J. A. Perman, B. J. Sikora, R. Q. Snurr, P. K. Thallapally, J. Tian, L. Wojtas and M. J. Zaworotko, Highly selective carbon dioxide uptake by [Cu(bpy-n)$_2$(SiF$_6$)] (bpy-1=4,4′-bipyridine; bpy-2=1,2-bis(4-pyridyl) ethene), *J. Am. Chem. Soc.*, 2012, **134**, 3663–3666.

41 L. Yang, X. Cui, Y. Zhang, Q. Yang and H. Xing, A highly sensitive flexible metal–organic framework sets a new benchmark for separating propyne from propylene, *J. Mater. Chem. A*, 2018, **6**, 24452–24458.

42 L. Li, L. Guo, F. Zheng, Z. Zhang, Q. Yang, Y. Yang, Q. Ren and Z. Bao, Calcium-Based Metal-Organic Framework for Simultaneous Capture of Trace Propyne and Propadiene from Propylene, *ACS Appl. Mater. Interfaces*, 2020, **12**, 17147–17154.

43 H.-M. Wen, L. Li, R.-B. Lin, B. Li, B. Hu, W. Zhou, J. Hu and B. Chen, Fine-tuning of nano-traps in a stable metal–organic framework for highly efficient removal of propyne from propylene, *J. Mater. Chem. A*, 2018, **6**, 6931–6937.

44 M. Khraisheh, F. AlMomani and G. Walker, High Purity/Recovery Separation of Propylene from Propyne Using Anion Pillared Metal-Organic Framework: Application of Vacuum Swing Adsorption (VSA), *Energies*, 2021, **14**, 609.

45 Z. T. Lin, Q. Y. Liu, L. Yang, C. T. He, L. Li and Y. L. Wang, Fluorinated Biphenyldicarboxylate-Based Metal-Organic Framework Exhibiting Efficient Propyne/Propylene Separation, *Inorg. Chem.*, 2020, **59**, 4030–4036.

46 Z. Zhang, Q. Ding, J. Cui, X. Cui and H. Xing, Fine-Tuning Pore Dimension in Hybrid Ultramicroporous Materials Boosting Simultaneous Trapping of Trace Alkynes from Alkenes, *Small*, 2020, **16**, e2005360.

47 X. Suo, H. Pan, L. Chen, X. Cui and H. Xing, Control of Functionalized Pore Environment in Robust Ionic Ultramicroporous Polymers for Efficient Removal of Trace Propyne from Propylene, *ACS Appl. Mater. Interfaces*, 2021, **13**, 42706–42714.

48 K.-J. Chen, R.-B. Lin, P.-Q. Liao, C.-T. He, J.-B. Lin, W. Xue, Y.-B. Zhang, J.-P. Zhang and X.-M. Chen, New Zn-Aminotriazolate-Dicarboxylate Frameworks: Synthesis, Structures, and Adsorption Properties, *Cryst. Growth Des.*, 2013, **13**, 2118–2123.

49 Materials Studio v5.5, Accelrys Inc., San Diego, CA, 2010.

50 A. L. Spek, Single-crystal structure validation with the program PLATON, *J. Appl. Crystallogr.*, 2003, **36**, 7–13.

51 Z. Li, L. Li, L. Guo, J. Wang, Q. Yang, Z. Zhang, Y. Yang, Z. Bao and Q. Ren, Gallate-Based Metal–Organic Frameworks for Highly Efficient Removal of Trace Propyne from Propylene, *Ind. Eng. Chem. Res.*, 2020, **59**, 13716–13723.

52 Y.-L. Peng, T. Wang, C. Jin, P. Li, S. Suepaul, G. Beemer, Y. Chen, R. Krishna, P. Cheng, T. Pham, B. Space, M. J. Zaworotko and Z. Zhang, A robust heterometallic ultramicroporous MOF with ultrahigh selectivity for

propyne/propylene separation, *J. Mater. Chem. A*, 2021, **9**, 2850–2856.
53 J.-P. Zhang and X.-M. Chen, Exceptional Framework Flexibility and Sorption Behavior of a Multifunctional Porous Cuprous Triazolate Framework, *J. Am. Chem. Soc.*, 2008, **130**, 6010–6017.
54 S. Ma, D. Sun, D. Yuan, X. Wang and H.-C. Zhou, Preparation and Gas Adsorption Studies of Three Mesh-Adjustable Molecular Sieves with a Common Structure, *J. Am. Chem. Soc.*, 2009, **131**, 6445–6451.
55 G. S. Pawley, Unit-Cell REFINEMENT FROM Powder Diffraction Scans, *J. Appl. Crystallogr.*, 1981, **14**, 357–361.
56 C. F. Macrae, I. Sovago, S. J. Cottrell, P. T. A. Galek, P. McCabe, E. Pidcock, M. Platings, G. P. Shields, J. S. Stevens, M. Towler and P. A. Wood, Mercury 4.0: from visualization to analysis, design and prediction, *J. Appl. Crystallogr.*, 2020, **53**, 226–235.
57 A. L. Myers and J. M. Prausnitz, Thermodynamics of mixed-gas adsorption, *AIChE J.*, 1965, **11**, 121–127.